Iran Polym J (2015) 24:29–40
DOI 10.1007/s13726-014-0297-9

ORIGINAL PAPER

Fabrication and characterization of mineralized P(LLA-CL)/SF three-dimensional nanoyarn scaffolds

Binbin Sun · Jun Li · Wei Liu · Bhutto M. Aqeel · Hany El-Hamshary · Salem S. Al-Deyab · Xiumei Mo

Received: 14 April 2014 / Accepted: 29 November 2014 / Published online: 16 December 2014

Abstract Particular attention has been given to three-dimensional scaffolds for bone tissue regeneration. In this study, poly(L-lactic acid-co-ε-caprolactone) (P(LLA-CL) nanoyarn scaffold and poly(L-lactic acid-co-caprolactone)/silk fibroin (P(LLA-CL)/SF) nanoyarn scaffold were fabricated by a dynamic liquid support electrospinning system; and then the three-dimensional (3D) nanoyarn scaffolds were prepared by freeze-drying processes. The results indicated the average diameter of P(LLA-CL) and P(LLA-CL)/SF nanoyarns were 29.44 ± 3.47 μm and 11.59 ± 0.46 μm, respectively. The yarn in the nanoyarn scaffold was twisted by many nanofibers as evidenced by scanning electron microscope (SEM) result. These nanoyarn scaffolds were biomineralized by alternatively immersing the nanoyarn scaffolds into phosphoric acid and calcium ion solutions. After biomineralization, the existence of hydroxyapatite (HA) particles on the scaffolds was confirmed using fourier transform infrared spectroscopy (FTIR) and X-ray diffraction (XRD) analysis. In vitro study of cell proliferation was found to be higher on P(LLA-CL)/SF scaffold as compared to P(LLA-CL) scaffold after culturing for 14 days. H&E staining results showed that cells not only attached to the surface of 3D scaffold but also infiltrated into the scaffold. This study indicated that the electrospun P(LLA-CL)/SF scaffold with nanostructure morphology could improve cell adhesion and proliferation and electrospun P(LLA-CL)/SF scaffold with biomineralization has a potential application for bone tissue engineering.

Keywords Nanoyarns · P(LLA-CL)/SF · Dynamic liquid support electrospinning · Biomineralization

B. Sun · J. Li · W. Liu · B. M. Aqeel · X. Mo (✉)
Biomaterials and Tissue Engineering Laboratory, College of Chemistry, Chemical Engineering and Bioengineering, Donghua University, Rm 4088 No.4 College Building, Shanghai 201620, People's Republic of China
e-mail: med@dhu.edu.cn

H. El-Hamshary · S. S. Al-Deyab · X. Mo
Department of Chemistry, College of Science, King Saud University, P.O. Box: 2455, Riyadh 11451, Kingdom of Saudi Arabia

H. El-Hamshary
Department of Chemistry, Faculty of Science, Tanta University, Tanta 31527, Egypt

Introduction

Bone is an organic–inorganic special, complex, and functional connective tissue which has a three-dimensional (3D) porous structure. The repair of bone defect was a big challenge for scientists [1]. There are several available methods to repair the bone defect in clinic, such as allograft, autograft, and xenograft. Autogenous iliac crest bone grafting is regarded as "gold standard". However, the morbidity of iliac crest bone harvesting includes chronic donor site pain, infection, fracture, hematoma, increased operation time and costs is reported to be as high as 30 %. With the development of tissue engineering, bone graft substitutes has emerged as a new way for bone defect treatment [2]. It is a promising way to repair bone defects by the combination of cells, biomaterial scaffolds, and bioactive factors [3, 4]. Many studies revealed that the artificial bone scaffold with nano-topological structure has a great potential for bone regeneration.

There is a 3D environment in human bone tissue for cells to attach, migrate, proliferate, and differentiate. Various methods have been developed to fabricate 3D porous

scaffold which mimics natural 3D extracellular matrix (ECM) environment. Thorvaldsson et al. [5] and Tzezana et al. [6] fabricated 3D nanofibrous scaffold by electrospinning and 3D multilayer nanofibrous scaffold by layered hydrospinning method. These scaffolds significantly improved cell adhesion and proliferation. A dynamic liquid supporting system was reported by Teo et al. [2], where they used a device to fabricate 3D nanoyarn scaffold by the power of a flow of water. Wu et al. [7] prepared P(LLA-CL)/SF nanoyarn scaffolds by this method, and they found that cells grew along the nanoyarns and infiltrated into the nanoyarn scaffolds.

Many synthetic and natural polymeric materials have been employed in bone tissue engineering. Poly(L-lactic acid-co-ε-caprolactone)[P(LLA-CL)], a synthetic polymer, has many advantages, such as good mechanical properties, no cytotoxicity and biodegradability [8]. Kim et al. [9] synthesized P(LLA-CL) scaffold by random copolymerization process and found the P(LLA-CL) film had good blood compatibility. Xu et al. [10] fabricated P(LLA-CL)/collagen nanoyarn scaffold for tendon tissue engineering. They found that the cells could infiltrate into the 3D scaffold after 14 days of cell culture. However, literature reveals that the surface of P(LLA-CL) scaffold lacks adhesive proteins and structural proteins which play important roles in cell adhesion, cell proliferation, and tissue remodeling [11, 12].

Study shows that natural materials, such as collagen, chitosan, and sodium alginate, have usually good biocompatibility [13]. Silk fibroin (SF) is a natural protein, it attracted more and more attention due to its unique properties [14, 15], i.e., good oxygen and water vapor permeability, biocompatibility, biodegradability, lower inflammatory response in the body, and low cost [16–18]. However, the mechanical property of SF is weak [19]. Studies showed that natural polymeric scaffold exhibited better biological properties than those of synthetic polymeric scaffold, and synthetic polymeric scaffolds have better mechanical properties than those of natural polymeric scaffolds [20, 21].

Bone ECM consists of two main components, one is organic collagen type I, and the other one is inorganic nanoscopic hydroxyapatite (HA) [22]. Rizzi et al. fabricated and mineralized the scaffold for bone tissue engineering. They found that the scaffold had a good biocompatibility and cell proliferation ability [23]. Biomimetic mineralization can attach inorganic HA on scaffold which enhance the biocompatibility and osteoconductivity of the scaffold [24–26]. Two main methods could be used for deposition of HA on the scaffold, treating the scaffold with simulated body fluid (SBF), and immersing the scaffold in $CaCl_2$ and Na_2HPO_4 solutions, alternatively. The alternative mineralization method is simple and the solutions for mineralization are easy to prepare.

The aim of this study is to fabricate 3D nanoyarn scaffold and evaluates its application in bone tissue engineering. P(LLA-CL)/SF nanoyarn scaffolds are fabricated by electrospinning of the dynamic liquid supporting system, while alternative mineralization method was used for deposition of HA on the 3D nanoyarn scaffolds. The morphology of the scaffolds was observed by SEM, whereas the physical and chemical structures were characterized by X-ray diffraction and Fourier transforms infrared spectroscopy, respectively. The biological properties of the 3D nanoyarn scaffolds were also investigated.

Experimental

Materials

A copolymer of poly(L-lactide-co-caprolactone) (P(LLA-CL)) (75:25), which has a composition of 75 mol% L-lactide, was supplied by Gunze limited Co. Ltd. (Japan). 1,1,1,3,3,3-hexafluoro-2-propanol (HFIP) was purchased from Daikin Industries Ltd. (Japan). Cocoons of *Bombyx mori* silkworm were kindly supplied by Jiaxing Silk Co. Ltd. (China). All culture media and reagents were purchased from Gibco Life Technologies Co., USA.

Preparation of SF and electrospinning solution

The silk fibroin (SF) was prepared following the previously published procedure [27]. Briefly, raw silk was degummed three times with 0.5 wt% Na_2CO_3 solution at 100 °C for 30 min and washed with distilled water. Then degummed silk was dissolved in $CaCl_2/H_2O/EtOH$ solution (molar ratio 1/8/2) at 70 °C for 1 h. The solution was dialyzed with cellulose tubular membrane (250-7u; Sigma) in distilled water for 3 days at room temperature. The water was changed every 4 h. The SF solution was filtered and freeze-dried to obtain the regenerated SF sponges.

P(LLA-CL) and silk fibroin were dissolved in 1,1,1,3,3,3-hexafluoro-2-propanol (HFIP) to yield an ultimate concentration of 8 wt% (w/v) with P(LLA-CL)/SF ratio of 1:1. The P(LLA-CL) electrospinning solution was prepared by the same method, and the prepared solution was constantly stirred overnight.

Scaffold fabrication

The prepared solutions of P(LLA-CL) and P(LLA-CL)/SF were used to fabricate scaffold that is shown in Fig. 1. In the first step (Fig. 1a), nanoyarns scaffold has been fabricated using the dynamic liquid supporting system as previously described [28]. In brief, the spinning solution was carried out by water cycling system, and the device

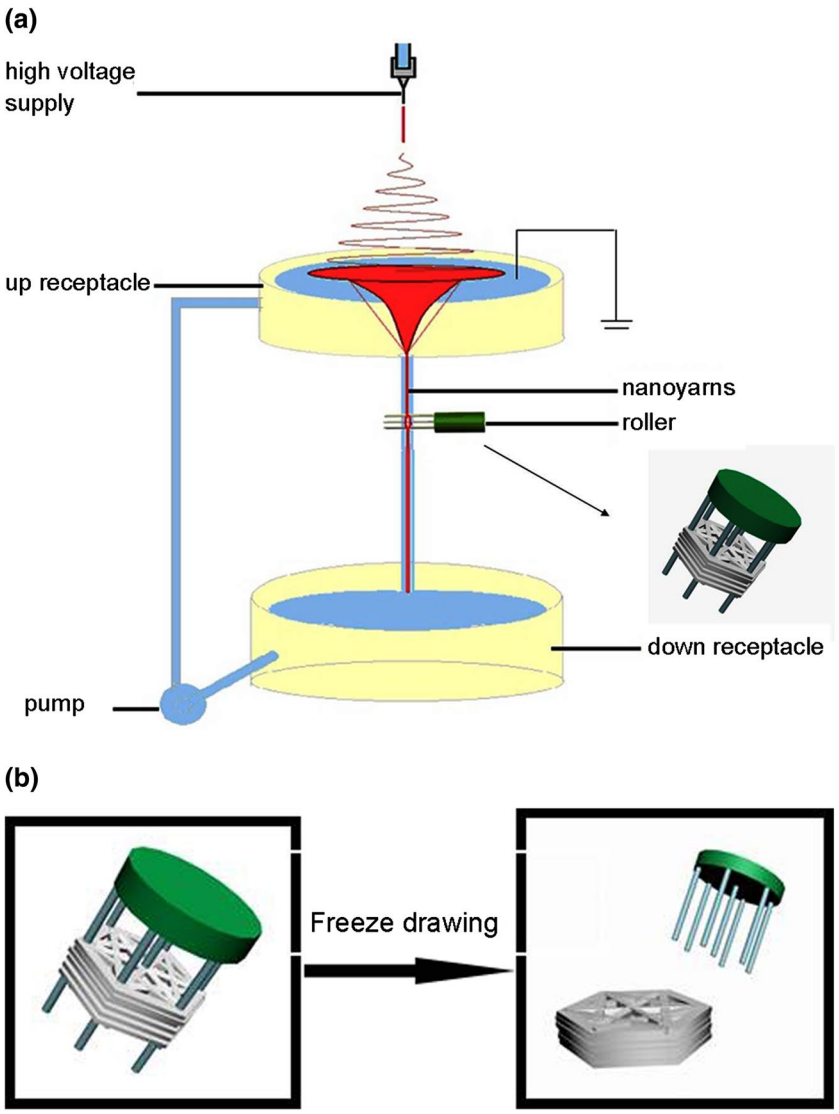

Fig. 1 Schematic of the electrospinning with a dynamic supporting system to fabricate nanoyarn scaffold. (Step 1) nanoyarns fabrication by electrospinning (**a**) and (Step 2) fiber reinforced scaffold fabrication and moving scaffold from the roller by freeze-drying technology (**b**)

consisted of two basins at top and bottom of the system. The drained water was deposited in the bottom basin and recycled to the top basin by a pump (2 L/min) (Shanghai Yi-Ling Pump Co. Ltd., China) to keep the water level constant in the basin. A plastic syringe equipped with a needle with an inner diameter of 1.2 mm and a seven-pin plug-like roller rotated in the flow water at a lower speed to collect nanoyarns. The blended solution jet rate, located 8–10 cm above the water vortex, was 0.8 mL/h under a high voltage of 14 kV. In the next step (Fig. 1 b), the prepared scaffold was put at −80 °C in a freezer-dryer for 2 h and then separated from the roller collector.

Scaffold biomineralization

The $CaCl_2$ (0.5 M and pH = 7.2) and Na_2HPO_4 (0.3 M and pH = 8.96) solutions were prepared using deionized water. The scaffold was biomimetic mineralized by immersing the scaffold in $CaCl_2$ solution for 1 min, and after rinsing with the deionized water again immersed with Na_2HPO_4 solution for 1 min to complete the one cycle. Mineralization processes were repeated for 3, 6, and 9 cycles to achieve different scaffolds.

Morphology

The structures and surface morphology of the prepared scaffolds were observed by FUJI-Z200 digital camera and scanning electron microscope (SEM) (TM-1000 (Hitachi, Japan)). Dry samples were sputter-coated with gold for 10 s (twice) before the scanning of SEM, the accelerating voltage was 10 kV. The average nanofiber diameters or nanoyarns were measured by Image J (National Institute of Health, USA). In order to determine the average diameters and distributions of the electrospun nanofibers and nanoyarns, 100 of randomly oriented nanofibers and nanoyarns

were chosen randomly to be measured from SEM micrographs, respectively.

Characterization

The prepared scaffolds characteristic were evaluated by both fourier transforms infrared spectroscopy (FTIR) and powder X-ray diffraction (XRD). Infrared measurements were performed on an Avatar 380 FTIR spectrometer, and XRD analysis was used a D/Max-2550 PC X-ray diffractometer (Rigaku, Japan) with Cu Kα radiation. In addition, the thermogravimetric (TG) properties of prepared scaffolds were characterized by using a thermal analyzer (TG-209-F1). In the experiment, argon was used as carrier gas with a flow rate of 50 mL/min, and the heating rate was controlled at 10 °C/min from room temperature to 600 °C.

Cell culture and seeding

Mouse pre-osteoblastic cells (MC3T3-E1) (Chinese Academy of Sciences, Shanghai, China) were cultured in Alpha Minimum Essential Medium containing 10 % fetal bovine serum and 1 % streptomycin/penicillin and maintained at 37 °C in a CO_2 incubator. The media were changed every other day.

The scaffolds were cut to a slice with 1 mm height and 14 mm diameter, placed into 24-well plates. The samples were sterilized in 75 % ethanol for 2 h, then washed with PBS and soaked in cell culture medium overnight. MC3T3-E1 were seeded at a density of 1.0×10^4 cells per well on different scaffolds. After 24 h, the media were supplemented with 10 mM β-glycerol phosphate and 50 mg/mL *L*-ascorbic acid (Sigma, St. Louis, MO). Cells were cultured for a period of 14 days.

Cell proliferation and infiltration

The experiment of MTT measured the cell viability and the cell proliferation at 3, 7, and 14 days post-seeding, respectively. Each test point has three parallel experiments. The plate was read at the absorbance of 570 nm using an enzyme-labeled instrument (MK3, Thermo, USA). Then, the results of experimental data were analyzed by Origin 7.5. *T* test was also conducted to find out the salient differences of cell proliferation in different scaffolds.

Cell infiltration studies on the scaffolds were performed using hematoxylin−eosin (H&E) stain. After 3, 7, and 14 days post-seeding, cell-scaffold constructs were removed form media and rinsed three times with PBS (5 min per wash) and fixed with 4 % (v/v) paraformaldehyde solution for 30 min and stained with H&E. Finally cell proliferation and cell infiltration were observed under an optical microscope (H600L, Nikon, Japan).

Cell morphologies on scaffolds

Cell morphology and the interaction between cells and scaffolds were studied by SEM at the 14th day of incubation. The culture media were removed from scaffolds by gently washing with PBS, and cells were fixed with 4 % (v/v) paraformaldehyde solution for 30 min at 4 °C. Then, the scaffolds were dehydrated using ethanol with concentrations of 30, 50, 70, 90, and 100 % (v/v), respectively, before being dried. Subsequently, they were coated with gold and imaged via SEM.

Results and discussion

Morphologies of scaffolds

The fabricated scaffolds were soaked in deionized water and freeze-dried at −80 °C. During this process, the scaffolds experienced a growth of ice crystal, vacuum drying, and sublimation, and resulted in a 3D scaffold. The optical images of P(LLA-CL) and P(LLA-CL)/SF scaffolds are shown in Fig. 2a and b, respectively. The structure of P(LLA-CL) scaffold is obviously different from that of P(LLA-CL)/SF scaffold. As can be seen, the macrostructure of P(LLA-CL) scaffold is smooth and regular on the roller collector, but the macrostructure of P(LLA-CL)/SF scaffold is random and very loose. It indicated that the addition of SF in electrospinning solution has affected the structure of P(LLA-CL)/SF scaffold.

SEM micrographs of nanoyarn scaffolds of P(LLA-CL) and P(LLA-CL)/SF are shown in Fig. 3a and b, respectively. It is demonstrated that the nanoyarn scaffolds consisted of many 3D porous structures. In our previous study, higher porosity provided space for cell to grow and adhere [18] and more importantly, the porous structure of the scaffold enhanced the nutrition transport. It was also noted that the morphology of P(LLA-CL) nanoyarns is smooth, which is due to the main chain of P(LLA-CL) molecules as single C–C bond and the molecular chain segments moved in a flexible way. The size of the P(LLA-CL)/SF scaffold is smaller than P(LLA-CL) scaffold due to the former shrinkage. This phenomenon could be explained by the increase of conductivity of the blend solution with increasing SF content. Silk fibroin is a typical amphiprotic macromolecule electrolyte, which composed of hydrophobic blocks with highly preserved repetitive sequence consisting of short side-chain amino acids, such as glycine and alanine, and hydrophilic blocks with more complex sequences that consist of larger side-chain amino acids as well as charged amino acids [29, 30]. When SF was employed, more ions were formed in the blend solution. The conductivity of the solution could increase through the addition of ions. On

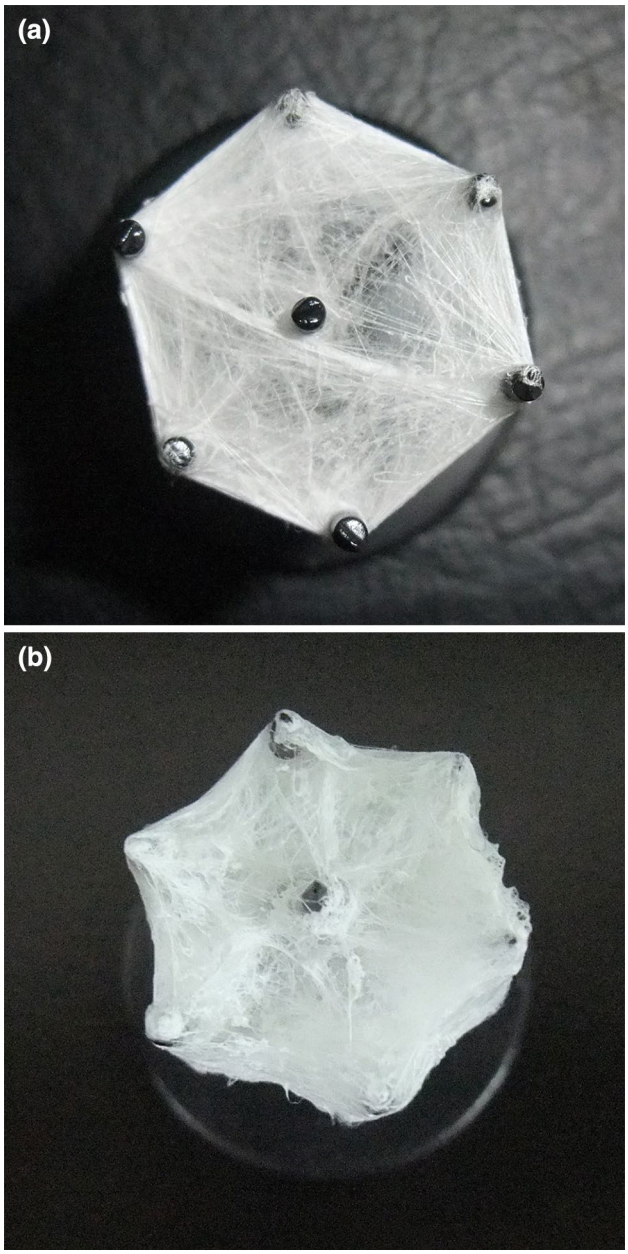

Fig. 2 Photos of P(LLA-CL) (**a**) and P(LLA-CL)/SF (**b**) scaffolds

the other hand, the increased charge density will increase elongational forces, which exert on the fiber jet to yield a smaller fiber. Thus, the P(LLA-CL)/SF scaffold looks shrunk.

A single nanoyarn was formed by 30–40 nanofibers by the force of water vortex. As shown in Fig. 3, the average diameter of P(LLA-CL) nanofibers was 1,021 ± 221 nm (Fig. 3c, e), and the average diameter of P(LLA-CL)/SF nanofibers was 313 ± 66 nm (Fig. 3d, f). The diameter of the P(LLA-CL) nanoyarn and P(LLA-CL)/SF was 29.44 ± 3.47 μm and 11.59 ± 0.46 μm, respectively. It was also observed that the diameter of P(LLA-CL)/SF scaffold is smaller than that of the P(LLA-CL) scaffold. It indicates that P(LLA-CL)/SF scaffold has higher porosity due to the smaller diameter of the nanoyarn. In addition, hydrophilic groups of SF are composed of larger side chains of amino acids [31]. These groups carry many of the same electric charges, thus, the repulsive force between these same electric charges were increased which produce smaller nanofibers of P(LLA-CL)/SF during the process of electrospinning.

Biomineralization of scaffolds

Figure 4 shows the mineralized nanoyarn scaffolds which were treated with phosphate and calcium solutions for 3 (Fig. 4a, b), 6 (Fig. 4c, d) and 9 cycles (Fig. 4e, f). It is noted that with the increasing number of cycles, the amount of HA increased on both P(LLA-CL) and P(LLA-CL)/SF scaffolds. Although the HA particles can improve the biocompatibility of the scaffold, too many HA particles can also reduce the porosity of the scaffold; therefore, the 6 cycles were the best for this study.

As can be seen, more HA particles were formed on P(LLA-CL)/SF scaffold as compared to P(LLA-CL) scaffold. Silk fibroin molecules containing 12 % serine acid, 1.9 % aspartic acid, and 1.4 % glutamic acid ensure many hydroxyl and carboxyl groups. Previous studies showed that HA particles were formed by the adsorption of Ca^{2+} ions [32, 33]. It might be one of the possible explanations for observing more HA particles on P(LLA-CL)/SF scaffold, which has many negative charged groups due to the addition of SF that adsorb Ca^{2+} ions.

FTIR analysis

Figure 5 shows the FTIR spectra (4,000–500 cm^{-1}) of raw SF and P(LLA-CL) and P(LLA-CL)/SF nanoyarns. There is a main absorption peak in raw SF and P(LLA-CL)/SF scaffold spectra at 3,295 cm^{-1}, which is corresponding to N–H stretching vibration and hydroxyl O–H stretching vibration of free amino groups. It reveals the existence of SF in P(LLA-CL)/SF scaffold. Two representative adsorption peaks at 3,069 and 2,938 cm^{-1} are corresponding to $–CH_3$ and $–CH_2$ stretching vibrations in raw SF, P(LLA-CL), and P(LLA-CL)/SF scaffold, respectively. P(LLA-CL) and P(LLA-CL)/SF scaffold have adsorption peaks at 1,756 and 1,757 cm^{-1} which are corresponding to C–O stretching [10].

There were three adsorption peaks noted at 1651, 1532, and 1237 cm^{-1} for raw SF, while the characteristic adsorption peaks of SF were 1650–1660, 1535–1545, and 1235–1240 cm^{-1}, which are an attribute of amide I, amide II, and amide II, respectively. The adsorption peak of amide I at 1,651 cm^{-1} shifted to 1,627 cm^{-1}, which

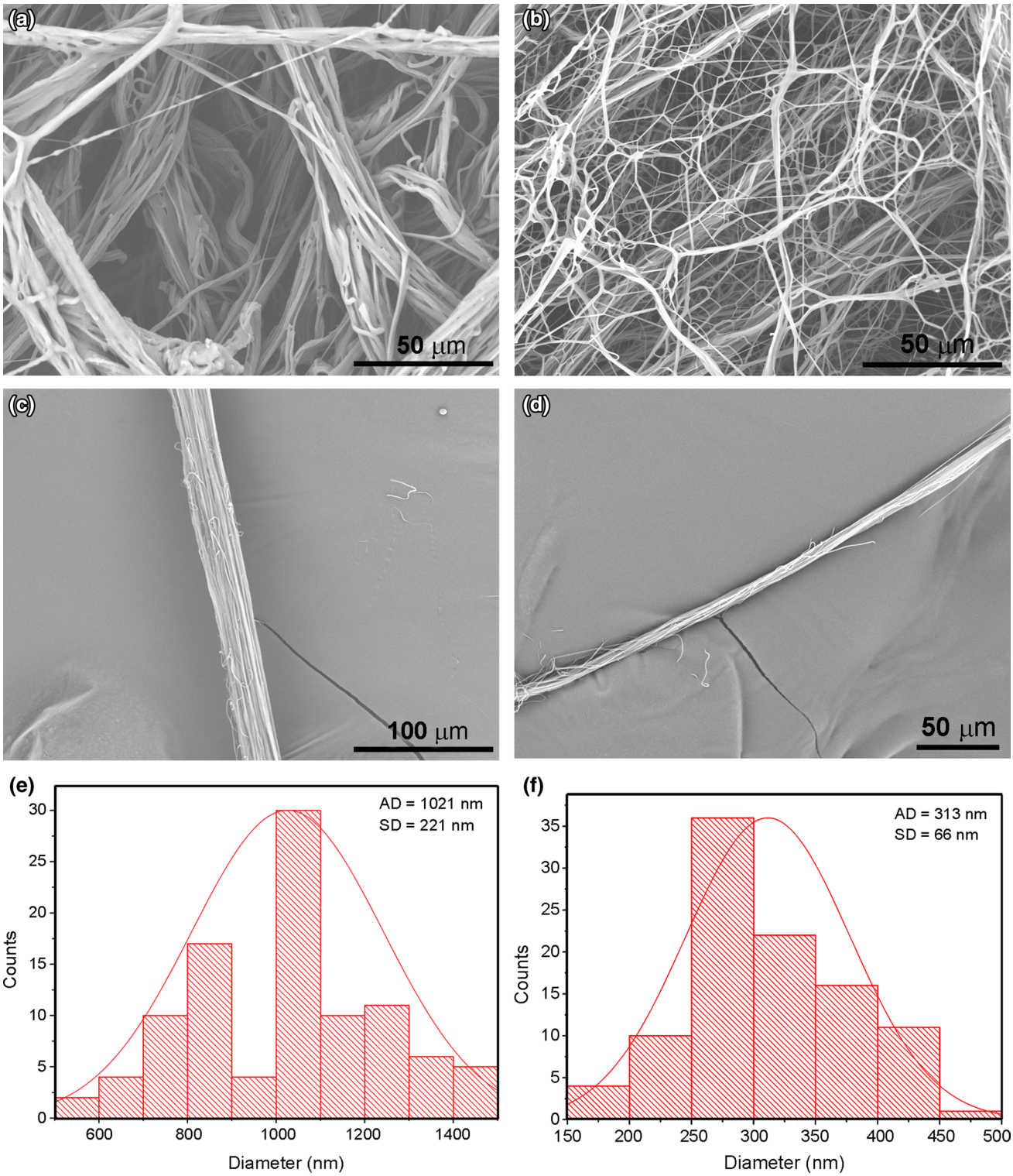

Fig. 3 SEM micrographs of P(LLA-CL) (**a**), P(LLA-CL)/SF (**b**), sub-thread P(LLA-CL) (**c**) and sub-thread P(LLA-CL)/SF (**d**), nanoyarns. Diameter distributions of P(LLA-CL) (**e**) and P(LLA-CL)/SF (**f**) nanoyarns

was attributed to the bond C = N and C–N by the cross-linking reaction. While P(LLA-CL) blend with SF shows characteristic adsorption peak of amide II shifted from 1,532 to 1,529 cm^{-1} which may be attributed to the change of conformation from random coils or α-helix to β-sheet [34]. Usually, the silk I crystalline structure

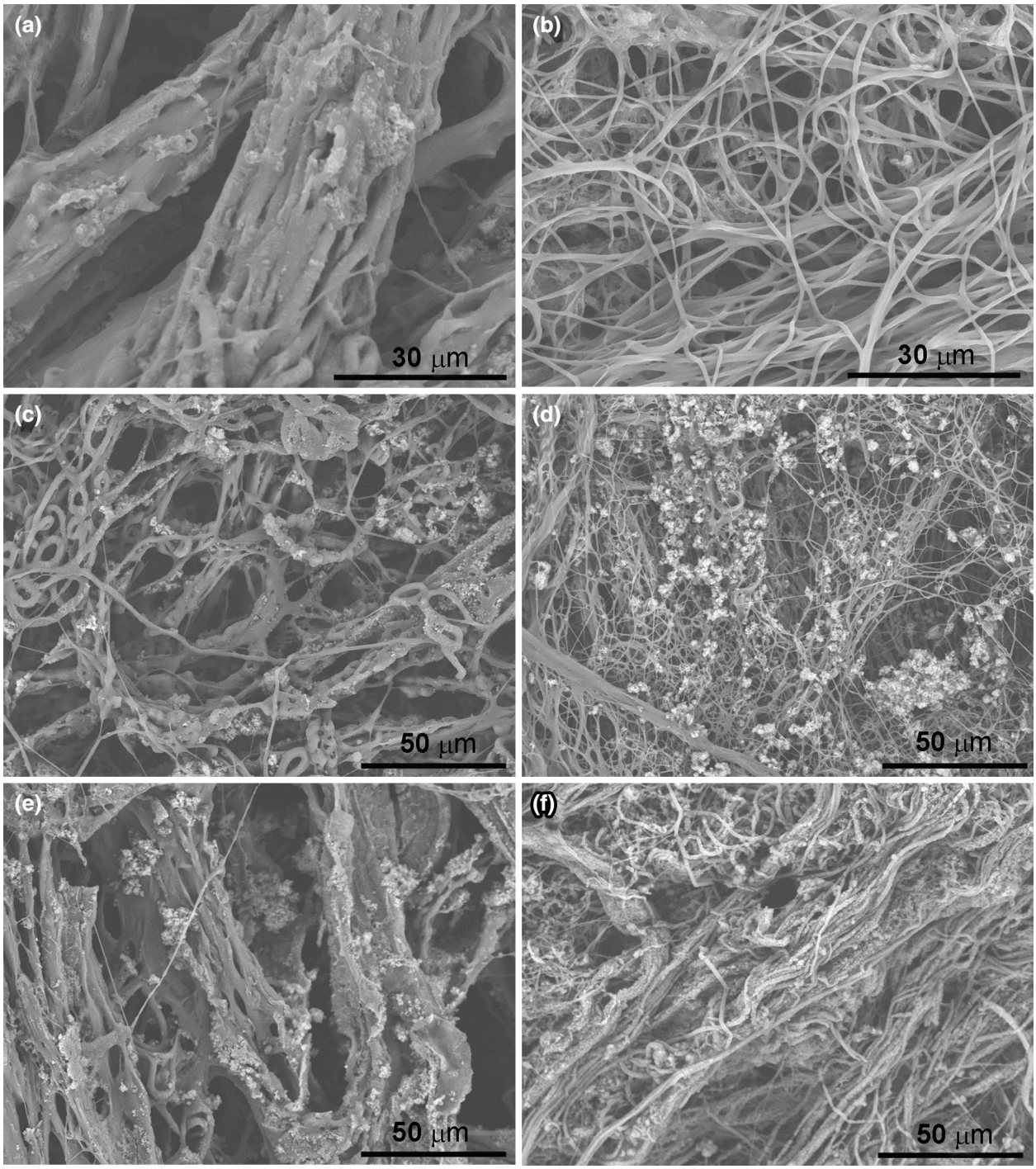

Fig. 4 SEM micrographs of biomineralized scaffolds of P(LLA-CL) and P(LLA-CL)/SF after 3 (**a** and **b**), 6 (**c** and **d**), and 9 (**e** and **f**) cycles, respectively

of high concentration SF is easy to dissolve in water by the influence of temperature and solvent, and further it transforms to silk II [35, 36]. Min et al. reported that the steam-made SF structure change from random coil conformation into β-folded structure [37]. In our case, the water penetrated into the middle of SF molecules and caused the rearrangement of SF structure.

The FTIR results of commercial HA, P(LLA-CL)-HA, and P(LLA-CL)/SF-HA nanoyarns are shown in Fig. 6. Characteristic absorption peak at 1,038 cm^{-1} is

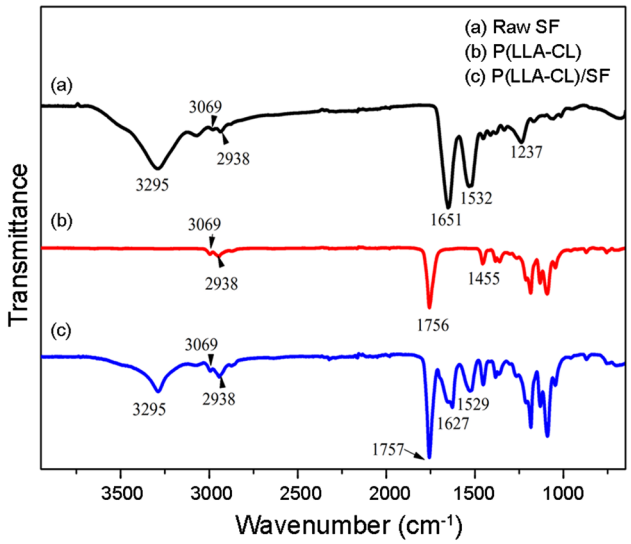

Fig. 5 FTIR spectra of raw SF and scaffolds of P(LLA-CL) and P(LLA-CL)/SF at 4,000–500 cm^{-1}

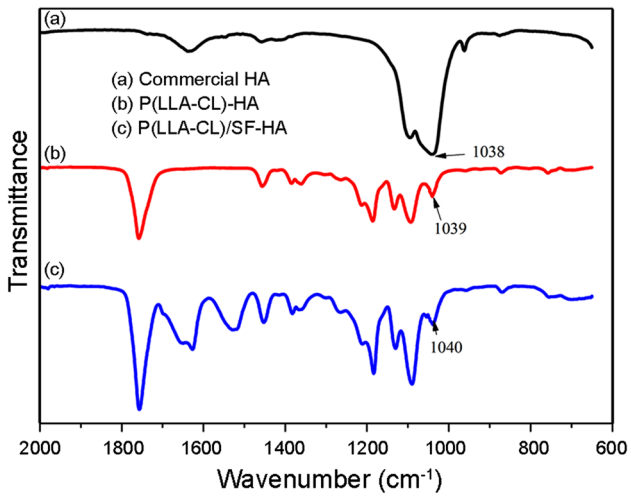

Fig. 6 FTIR spectra of commercial HA and nanoyarns of P(LLA-CL)-HA and P(LLA-CL)/SF-HA at 2,000–600 cm^{-1}

corresponding to PO_4^{3-} groups in commercial HA FTIR spectra [38, 39]. The same adsorption peaks are observed in the spectra of the P(LLA-CL)-HA and P(LLA-CL)/SF-HA scaffolds which proves the presence of HA on the mineralized scaffolds.

XRD analysis

The XRD patterns of P(LLA-CL), P(LLA-CL)/SF, P(LLA-CL)-HA, and P(LLA-CL)/SF-HA scaffolds are shown in Fig. 7. Previous study showed that the specific diffraction peaks of HA are located at 26° and 32° [40]. Figure 7 shows that there is a peak at 32° for

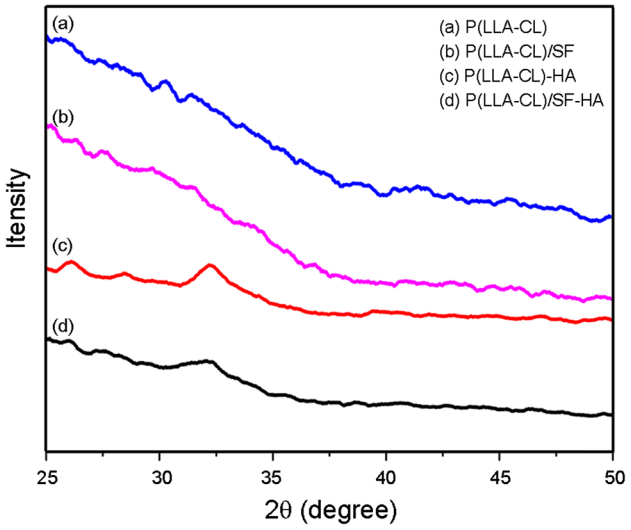

Fig. 7 XRD patterns of P(LLA-CL) (**a**), P(LLA-CL)/SF (**b**), P(LLA-CL)-HA(**c**), and P(LLA-CL)/SF-HA (**d**) scaffolds

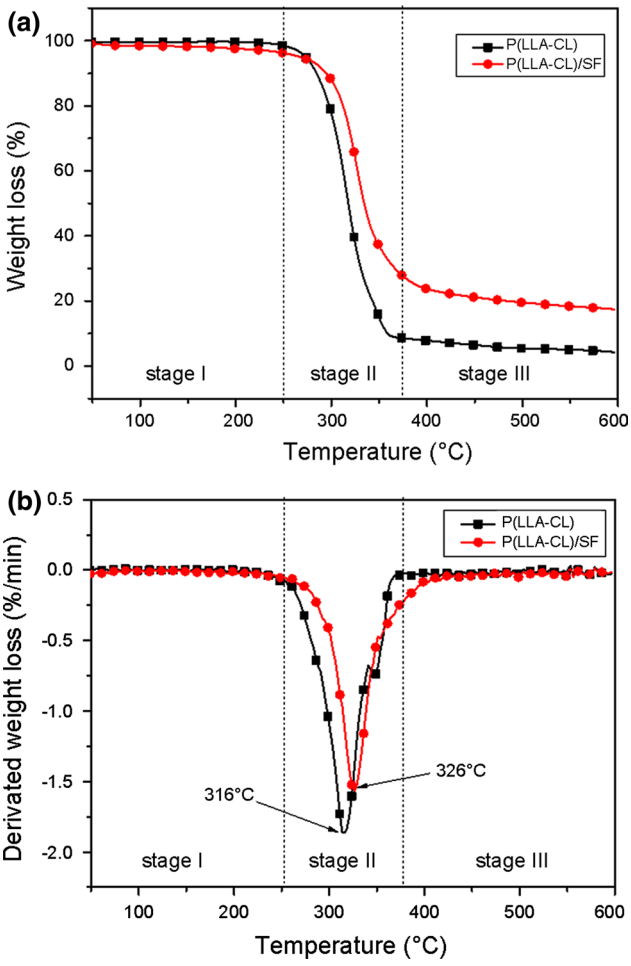

Fig. 8 TG curves (**a**) and DTG carves (**b**) of P(LLA-CL)/SF, and P(LLA-CL) scaffolds

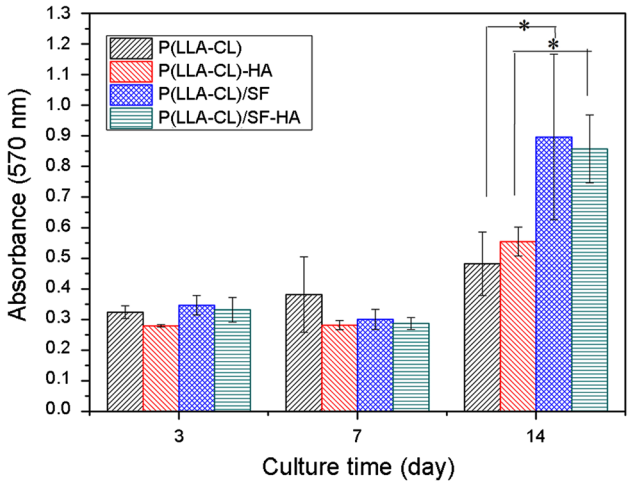

Fig. 9 Proliferation of MC3T3-E1 cells on P(LLA-CL), P(LLA-CL)/SF, P(LLA-CL)-HA, and P(LLA-CL)/SF-HA scaffolds at 3, 7, and 14 days, respectively

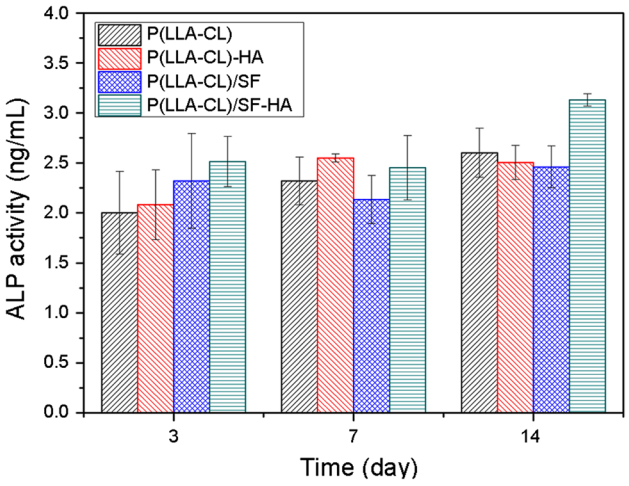

Fig. 10 ALP activity of MC3T3-E1 cells on P(LLA-CL), P(LLA-CL)/SF, P(LLA-CL)-HA, and P(LLA-CL)/SF-HA scaffolds at 3, 7, and 14 days, respectively

P(LLA-CL)-HA and P(LLA-CL)/SF-HA scaffolds which indicated that HA particles were deposited on the scaffolds.

Thermogravimetric analysis

TG is a method for determination of polymer thermal stability which has a close relationship with polymer molecule structure, degree of crystallinity, molecule size, molecule distribution, and so on. The TG curves of P(LLA-CL) and P(LLA-CL)/SF nanoyarns can be divided into three stages (Fig. 8a). It was found that the main weight loss occurred in stage II (250–380 °C) for P(LLA-CL) and P(LLA-CL)/SF scaffolds. Whereas, the weight loss ratio of P(LLA-CL) scaffold was 89 % which was higher than that of P(LLA-CL)/SF scaffold (66 %). The result corresponds to the DTG results (Fig. 8b). The temperatures of maximum weight loss of two samples were 316 and 326 °C, respectively. P(LLA-CL)/SF scaffold has better thermal stability than that of P(LLA-CL) counterpart.

Proliferation behavior of MC3T3-E1 cells

Figure 9 shows the proliferation of MC3T3-E1 cells on four nanoyarns scaffolds by MTT assay after 3, 7, and 14 days of cell culture. It indicated that there were no significant differences in the number of cells between the groups after 3 and 7 days of cell culture. However, The cell proliferation on P(LLA-CL)/SF scaffold was significantly higher than that on P(LLA-CL)/SF-HA scaffold at 14 days ($P > 0.05$). It is observed that the cell proliferation on the 3D scaffold was increased with the increase of the incubation time, which indicated the good biocompatibility of the scaffold. In addition, the cell proliferation on P(LLA-CL)/SF and P(LLA-CL)/SF-HA scaffolds was significantly higher than that on the P(LLA-CL) and P(LLA-CL)-HA scaffolds at 14th day ($P > 0.05$). It was earlier reported that the functional groups of SF could promote cell adhesion and proliferation [17, 18]. In the present study, the higher proliferation of cells on P(LLA-CL)/SF and P(LLA-CL)/SF-HA after 14 days of incubation might contribute to the functional groups of SF molecules.

ALP is an osteogenic marker for differentiation that is important for the construction of bone tissue matrix [41]. As shown in Fig. 10, the ALP activity of P(LLA-CL)/SF-HA scaffold was higher than that of the P(LLA-CL)/SF scaffold at 3, 7, and 14 days. It is indicated that deposition of HA on P(LLA-CL)/SF improves the osteoconductivity of P(LLA-CL)/SF scaffold.

Morphological and H&E staining of MC3T3-E1 cells on the scaffolds

Figure 11 shows H&E staining of cells on P(LLA-CL), P(LLA-CL)/SF, P(LLA-CL)-HA. and P(LLA-CL)/SF-HA scaffolds. It indicated that the cells grew well on the 3D scaffolds, and they infiltrated into the nanoyarn scaffolds as well. Due to highly porous structure, cells were attached on the nanoyarn scaffold surface and migrated into the inner pores of the scaffolds.

The morphology of the cells on four scaffolds was observed by SEM, as shown in micrographs e–h in Fig. 11.

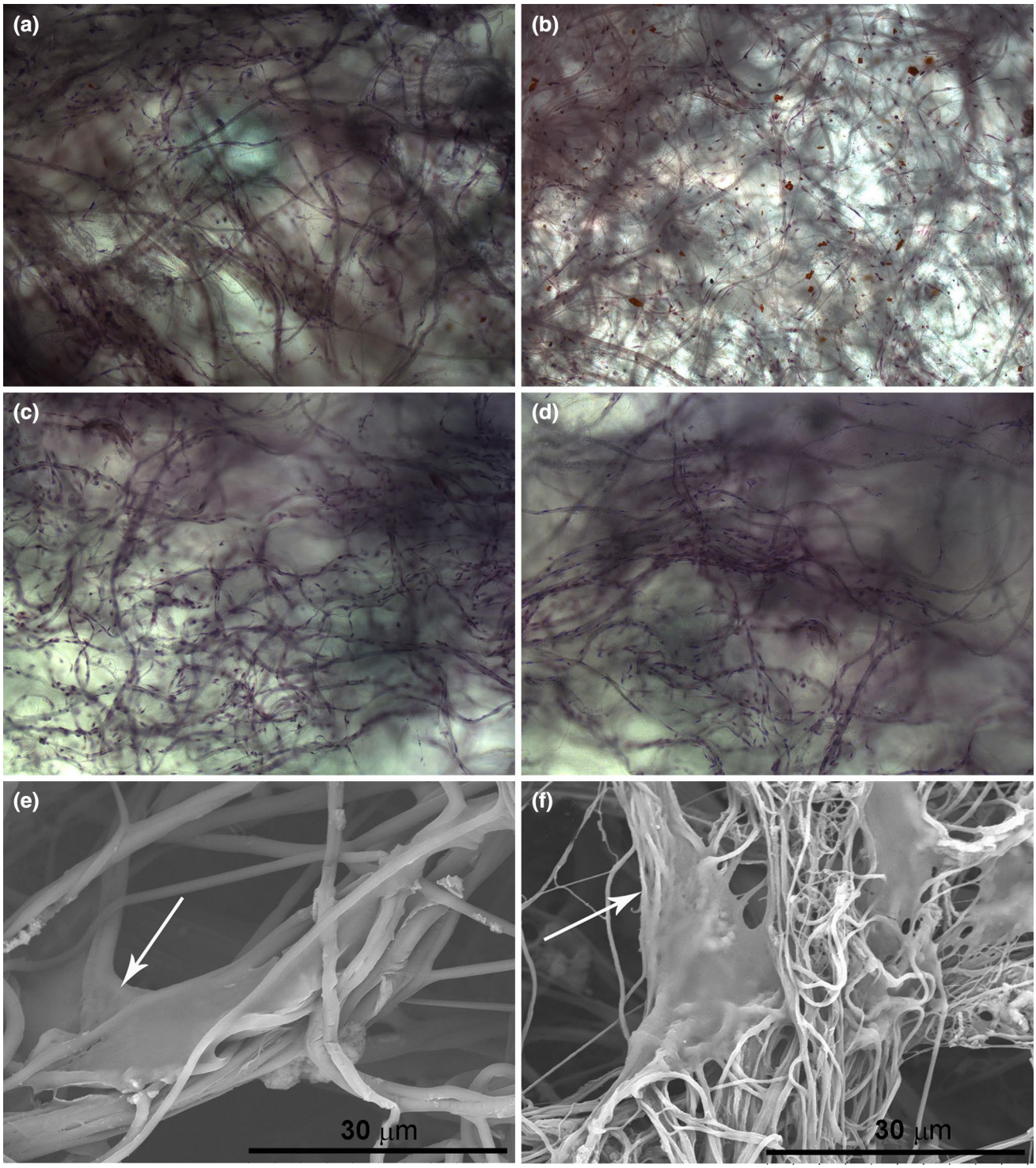

Fig. 11 The H&E staining images of cells on P(LLA-CL) (**a**), P(LLA-CL)/SF (**b**), P(LLA-CL)-HA (**c**) and P(LLA-CL)/SF-HA (**d**) scaffolds, and SEM micrographs of cells on P(LLA-CL) (**e**), P(LLA-CL)/SF (**f**), P(LLA-CL)-HA (**g**) and P(LLA-CL)/SF-HA (**h**) scaffolds. (Cells in the SEM micrographs have been labeled by *white arrow)*

It observed that MC3T3-E1 cells have extended their cytoplasm along the nanoyarn. These results suggested that the nanoyarn scaffolds have good biocompatibility. In addition, good cell infiltration indicated the porous nature of scaffold which provides enough space and 3D environment for cells' growth and immigration.

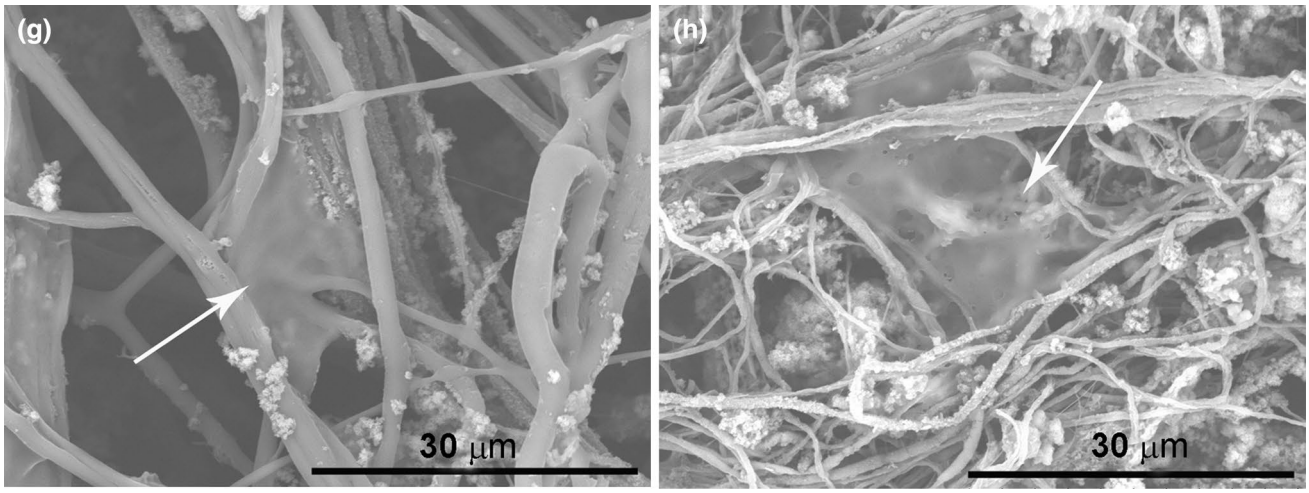

Fig. 11 continued

Conclusion

In this study, P(LLA-CL) and P(LLA-CL)/SF 3D nanoyarn scaffolds were fabricated by a dynamic liquid support electrospinning system. It was observed that P(LLA-CL)/SF nanoyarns have smaller diameter than P(LLA-CL) nanoyarns. The porous structure of the nanoyarn scaffold provided natural 3D environment for cells to infiltrate into it. The deposition of HA on P(LLA-CL)/SF improved the proliferation of cells and the osteoconductivity of nanoyarn scaffolds. All the above results suggest that the mineralized 3D porous P(LLA-CL)/SF nanoyarns scaffold have a great potential application in bone tissue engineering.

Acknowledgments This research was supported by Open Funding Project of the State Key Laboratory of Bioreactor Engineering, Science and Technology Commission of Shanghai Municipality Program (11nm0506200), National Nature Science Foundation of China (Project No. 31470941, 31271035), Deanship of Scientific Research at King Saud University research group project no. RGP-201.

References

1. Helsen JA, Jürgen Breme H (1998) Metals as biomaterials. Wiley, New York
2. Teo W, Liao S, Chan C, Ramakrishna S (2011) Fabrication and characterization of hierarchically organized nanoparticle-reinforced nanofibrous composite scaffolds. Acta Biomater 7:193–202
3. Burg KJL, Porter S, Kellam JF (2000) Biomaterial developments for bone tissue engineering. Biomaterials 21:2347–2359
4. Rose FRAJ, Oreffo ROC (2002) Bone tissue engineering: hope vs hype. Biochem Biophys Res Commun 292:1–7
5. Thorvaldsson A, Stenhamre H, Gatenholm P, Walkenström P (2008) Electrospinning of highly porous scaffolds for cartilage regeneration. Biomacromolecules 9:1044–1049
6. Tzezana R, Zussman E, Levenberg S (2008) A layered ultraporous scaffold for tissue engineering, created via a hydrospinning method. Tissue Eng Part C 14:281–288
7. Wu J, Liu S, He L, Wang H, He C, Fan C, Mo X (2012) Electrospun nanoyarn scaffold and its application in tissue engineering. Mater Lett 89:146–149
8. Sabir MI, Xu X, Li L (2009) A review on biodegradable polymeric materials for bone tissue engineering applications. J Mater Sci 44:5713–5724
9. Kim SI, Lim JI, Jung Y, Mun CH, Kim JH, Kim SH (2013) Preparation of enhanced hydrophobic poly(l-lactide-co-ε-caprolactone) films surface and its blood compatibility. Appl Surf Sci 276:586–591
10. Xu Y, Wu J, Wang H, Li H, Di N, Song L, Li S, Li D, Xiang Y, Liu W, Mo X, Zhou Q (2013) Fabrication of electrospun poly(L-lactide-co-ε-caprolactone)/collagen nanoyarn network as a novel, three-dimensional, macroporous, aligned scaffold for tendon tissue engineering. Tissue Eng Part C 19:925–936
11. Vaquette C, Kahn C, Frochot C, Nouvel C, Six JL, De Isla N, Luo LH, Cooper-White J, Rahouadj R, Wang X (2010) Aligned poly (L-lactic-co-ε-caprolactone) electrospun microfibers and knitted structure: a novel composite scaffold for ligament tissue engineering. J Biomed Mater Res A 94:1270–1282
12. Fang Z, Fu W, Dong Z, Zhang X, Gao B, Guo D, He H, Wang Y (2011) Preparation and biocompatibility of electrospun poly (L-lactide-co-ε-caprolactone)/fibrinogen blended nanofibrous scaffolds. Appl Surf Sci 257:4133–4138
13. Zheng L, Lu HQ, Fan HS, Zhang XD (2013) Reinforcement and chemical cross-linking in collagen-based scaffolds in cartilage tissue engineering: a comparative study. Iran Polym J 22:833–842
14. Fan H, Liu H, Toh SL, Goh JCH (2009) Anterior cruciate ligament regeneration using mesenchymal stem cells and silk scaffold in large animal model. Biomaterials 30:4967–4977
15. Liu H, Fan H, Wang Y, Toh SL, Goh JCH (2008) The interaction between a combined knitted silk scaffold and microporous silk sponge with human mesenchymal stem cells for ligament tissue engineering. Biomaterials 29:662–674
16. Meinel L, Hofmann S, Karageorgiou V, Kirker-Head C, McCool J, Gronowicz G, Zichner L, Langer R, Vunjak-Novakovic G, Kaplan DL (2005) The inflammatory responses to silk films in vitro and in vivo. Biomaterials 26:147–155

17. Horan RL, Antle K, Collette AL, Wang Y, Huang J, Moreau JE, Volloch V, Kaplan DL, Altman GH (2005) In vitro degradation of silk fibroin. Biomaterials 26:3385–3393
18. Zhang K, Wang H, Huang C, Su Y, Mo X, Ikada Y (2010) Fabrication of silk fibroin blended P(LLA-CL) nanofibrous scaffolds for tissue engineering. J Biomed Mater Res A 93:984–993
19. Muthumanickkam A, Subramanian S, Goweri M, Beaula WS, Ganesh V (2013) Comparative study on eri silk and mulberry silk fibroin scaffolds for biomedical applications. Iran Polym J 22:143–154
20. Kuo CK, Marturano JE, Tuan RS (2010) Novel strategies in tendon and ligament tissue engineering: advanced biomaterials and regeneration motifs. Sports Med Arthrosc Rehabil Ther Thecnol 2:20
21. Liu H, Fan H, Toh SL, Goh JC (2008) A comparison of rabbit mesenchymal stem cells and anterior cruciate ligament fibroblasts responses on combined silk scaffolds. Biomaterials 29:1443–1453
22. Olszta MJ, Cheng X, Jee SS, Kumar R, Kim YY, Kaufman MJ, Douglas EP, Gower LB (2007) Bone structure and formation: a new perspective. Mat Sci Eng R 58:77–116
23. Rizzi SC, Heath D, Coombes A, Bock N, Textor M, Downes S (2001) Biodegradable polymer/hydroxyapatite composites: surface analysis and initial attachment of human osteoblasts. J Biomed Mater Res 55:475–486
24. Bradt JH, Mertig M, Teresiak A, Pompe W (1999) Biomimetic mineralization of collagen by combined fibril assembly and calcium phosphate formation. Chem Mater 11:2694–2701
25. Xu AW, Ma Y, Cölfen H (2007) Biomimetic mineralization. J Mater Chem 17:415–449
26. Calvert P, Rieke P (1996) Biomimetic mineralization in and on polymers. Chem Mater 8:1715–1727
27. Nazarov R, Jin HJ, Kaplan DL (2004) Porous 3-D scaffolds from regenerated silk fibroin. Biomacromolecules 5:718–726
28. Teo WE, Gopal R, Ramaseshan R, Fujihara K, Ramakrishna S (2007) A dynamic liquid support system for continuous electrospun yarn fabrication. Polymer 48:3400–3405
29. Yin A, Zhang K, McClure MJ, Huang C, Wu J, Fang J, Mo X, Bowlin GL, Al-Deyab SS, El-Newehy M (2013) Electrospinning collagen/chitosan/poly (L-lactic acid-co-ε-caprolactone) to form a vascular graft: mechanical and biological characterization. J Biomed Mater Res A 101:1292–1301
30. Vepari C, Kaplan DL (2007) Silk as a biomaterial. Prog Polym Sci 32:991–1007
31. Wang Y, Kim HJ, Vunjak-Novakovic G, Kaplan DL (2006) Stem cell-based tissue engineering with silk biomaterials. Biomaterials 27:6064–6082
32. Tanahashi M, Matsuda T (1997) Surface functional group dependence on apatite formation on self-assembled monolayers in a simulated body fluid. J Biomed Mater Res 34:305–315
33. Sato K, Kumagai Y, Tanaka J (2000) Apatite formation on organic monolayers in simulated body environment. J Biomed Mater Res 50:16–20
34. Zhang K, Qian Y, Wang H, Fan L, Huang C, Yin A, Mo X (2010) Genipin-crosslinked silk fibroin/hydroxybutyl chitosan nanofibrous scaffolds for tissue-engineering application. J Biomed Mater Res A 95:870–881
35. Chen X, Shao Z, Marinkovic NS, Miller LM, Zhou P, Chance MR (2001) Conformation transition kinetics of regenerated *Bombyx mori* silk fibroin membrane monitored by time-resolved FTIR spectroscopy. Biophys Chem 89:25–34
36. Zhou P, Li G, Shao Z, Pan X, Yu T (2001) Structure of *Bombyx mori* silk fibroin based on the DFT chemical shift calculation. J Phys Chem B 105:12469–12476
37. Min BM, Jeong L, Lee KY, Park WH (2006) Regenerated silk fibroin nanofibers: water vapor-induced structural changes and their effects on the behavior of normal human cells. Macromol Biosci 6:285–292
38. Takeuchi A, Ohtsuki C, Miyazaki T, Tanaka H, Yamazaki M, Tanihara M (2003) Deposition of bone-like apatite on silk fiber in a solution that mimics extracellular fluid. J Biomed Mater Res A 65:283–289
39. Kawashita M, Nakao M, Minoda M, Kim HM, Beppu T, Miyamoto T, Kokubo T, Nakamura T (2003) Apatite-forming ability of carboxyl group-containing polymer gels in a simulated body fluid. Biomaterials 24:2477–2484
40. Mavis B, Demirtaş TT, Gümüşderelioğlu M, Gündüz G, Çolak Ü (2009) Synthesis, characterization and osteoblastic activity of polycaprolactone nanofibers coated with biomimetic calcium phosphate. Acta Biomater 5:3098–3111
41. Ngiam M, Liao S, Patil AJ, Cheng Z, Chan CK, Ramakrishna S (2009) The fabrication of nano-hydroxyapatite on PLGA and PLGA/collagen nanofibrous composite scaffolds and their effects in osteoblastic behavior for bone tissue engineering. Bone 45:4–16